Plant Physiol. (1989) 90, 1322–1328
0032-0889/89/90/1322/07/$01.00/0

Received for publication December 5, 1988
and in revised form March 14, 1989

Partitioning of Noncyclic Photosynthetic Electron Transport to O_2-Dependent Dissipative Processes as Probed by Fluorescence and CO_2 Exchange

Richard B. Peterson

Department of Biochemistry and Genetics, The Connecticut Agricultural Experiment Station, P.O. Box 1106, New Haven, Connecticut 06504

ABSTRACT

The partitioning of noncyclic photosynthetic electron transport between net fixation of CO_2 and collective O_2-dependent, dissipative processes such as photorespiration has been examined in intact leaf tissue from *Nicotiana tabacum*. The method involves simultaneous application of CO_2 exchange and pulse modulated fluorescence measurements. As either irradiance or CO_2 concentration is varied at 1% O_2 (*i.e.* absence of significant O_2-dependent electron flow), the quantum efficiency of PSII electron transport (Φ_{se}) with CO_2 as the terminal acceptor is a linear function of the ratio of photochemical:nonphotochemical fluorescence quenching coefficients (*i.e.* q_Q:q_{NP}). When the ambient O_2 concentration is raised to 20.5% or 42% the q_Q:q_{NP} is assumed to predict the quantum efficiency of total noncyclic electron transport (Φ'_{se}). A factor which represents the proportion of electron flow diverted to the aforementioned dissipative processes is calculated as ($\Phi'_{se} - \Phi_{se}$)/Φ'_{se} where Φ_{se} is now the observed quantum efficiency of electron transport in support of net fixation of CO_2. Examination of changes in electron allocation with CO_2 and O_2 concentration and irradiance at 25°C provides a test of the applicability of the Rubisco model to photosynthesis *in vivo*.

Chl fluorescence studies have long contributed substantially to our understanding of photosynthesis in higher plants. This is due to the specificity of fluorescence for the photosynthetic apparatus, easy detectability, and nonintrusive character. Changes in the intensity of variable fluorescence from PSII are generally interpreted in terms of processes that quench it relative to the maximum possible fluorescence yield for the sample. Quenching may be both 'photochemical' and 'nonphotochemical' in nature and expressed as coefficients q_Q[1] and q_{NP}, respectively (15). Photochemical quenching pertains to the redox state of the first stable quinone electron acceptor in PSII, *i.e.* Q_A. Nonphotochemical quenching is dominated by, although not limited to, dissipation of radiant energy as heat at the PSII reaction center and antennae pigment complex. Modulation techniques have enabled simultaneous separation and quantitation of these quenching processes (1, 4, 12, 23).

As an early electron acceptor in PSII, the degree of reduction of Q_A (*i.e.* $1 - q_Q$) is likely to reflect the availability of terminal electron acceptor relative to the density of excitation. Numerous studies have noted a positive, yet frequently nonlinear, relationship between quantum efficiency of photosynthesis and q_Q (12, 14, 22, 24). Accompanying changes in q_{NP} are likely to be at least partially responsible for this nonlinearity. Indeed, Weis and Berry (24) have described a linear decline in the quantum efficiency of open (*i.e.* Q_A oxidized) PSII reaction centers as nonphotochemical quenching increases in sunflower and bean leaves. Peterson *et al.* (22) reported a linear relationship between quantum efficiency and the ratio of q_Q:q_{NP} in spinach leaf tissue.

The relationships between quantum efficiency of photosynthesis and fluorescence quenching described above were performed at a low [O_2] so that effectively all of the photosynthetic electron transport was devoted to net fixation of CO_2. Elevated levels of O_2 in the gas phase will result in a diversion of a portion of the electron flow away from net uptake of CO_2 and toward photorespiratory processes such as refixation of CO_2 and NH_3 and reduction to triose phosphate of FGA produced by oxygenation of RuBP and metabolism of glycolate (6, 21, 25). Direct reduction of O_2 via Mehler processes could also occur (20). One may, however, propose that the ultimate partitioning of electron transport among these processes does not influence the inherent relationship among PSII quantum efficiency, q_Q, and q_{NP}.

In this report, I describe simultaneous measurements of CO_2 exchange and fluorescence at 1% O_2 that extend studies of q_Q, q_{NP}, and quantum efficiency of noncyclic electron transport to tobacco leaf tissue. Similar determinations were conducted at elevated O_2 concentrations and over a wide range of intercellular CO_2 levels. Under such conditions the difference between total electron transport as predicted by the ratio of q_Q:q_{NP} and that supporting net fixation of CO_2 is collectively ascribed to dissipative processes such as photorespiration and direct photoreduction of O_2. Observed changes in the partitioning of photosynthetic electron transport to dissipative processes are examined with regard to those expected based on the RuBP carboxylase/oxygenase (Rubisco) model as described previously (2, 6, 13, 17, 21).

MATERIALS AND METHODS

Plant Material

Nicotiana tabacum var Havana Seed was grown in a greenhouse in pots containing a commercial sphagnum moss:

[1] Abbreviations: q_Q, photochemical quenching coefficient; q_{NP}, nonphotochemical quenching coefficient; PGA, 3-phosphoglyceric acid; Φ_s, observed quantum efficiency of CO_2 fixation; Φ_{se}, $4 \times \Phi_s$; Φ'_{se}, predicted quantum efficiency of noncyclic photosynthetic electron transport; RuBP, ribulose bisphosphate; C_i, intercellular [CO_2] (μbars); Rubisco, ribulose-1,5-bisphosphate carboxylase/oxygenase.

perlite:vermiculite mixture (ProMix BX) and cultured weekly with a solution of 20-20-20 (N-P-K) fertilizer and Hoagland micronutrients. Fully expanded leaves were excised and washed carefully with hand soap followed by thorough rinsing with distilled H_2O. A 5 cm diameter leaf disc was cut from the leaf avoiding the midvein and was mounted in the Leaf Section Chamber (Analytical Development Co., Hoddesdon, U.K.). The remainder of the leaf was stored in the dark with the base immersed in H_2O.

CO_2 Exchange

Measurements of rates of CO_2 assimilation and transpiration at a leaf temperature of 25°C were performed using an open, flow-through system. The CO_2 and H_2O vapor concentration differentials were determined separately by IRGA (Beckman model 865, CO_2 and H_2O Analyzers, Fullerton, CA). The flow rate of the flushing gas was 2.0 L min^{-1}. The H_2O vapor concentration (*i.e.* dew point) of the flushing gas was set by bubbling through warm distilled H_2O followed by passage through a condenser immersed in a thermostatically controlled water bath. Gas phase (*i.e.* combined boundary layer and stomatal) conductances to H_2O and CO_2 and intercellular CO_2 concentration (C_i) were calculated as described (18). The boundary layer conductance to H_2O vapor was 0.68 mols H_2O m^{-2} s^{-1}. The H_2O vapor pressure deficit for the leaf sample was always ≤10 mbars.

Fluorescence Measurements

The PAM 101 Fluorescence Measuring System (H. Walz, Effeltrich, F. R. G.) was employed essentially as described previously (4, 22, 23) to measure variable fluorescence yield. White, actinic illumination was provided by a KL 1500 light source (Schott, Weisbaden, F.R.G.). Saturating pulses (700 ms) of white light (7500 μmol photons m^{-2} s^{-1}) were activated by a PAM 103 Trigger Control Unit at intervals of 100 s. The photochemical fluorescence quenching coefficient (q_Q) was given by $(F_s - F)/(F_s - F_o)$ where F is the steady state yield of fluorescence during actinic illumination, F_s is the maximum yield during the superimposed saturating flash, and F_o is the yield during a brief (2–4 s) dark interval imposed between the flashes. Likewise, the formula for the nonphotochemical quenching coefficient is given by $q_{NP} = (F_m - F_s)/(F_m - F_o)$. The maximal fluorescence yield (F_m) was determined at the end of each experiment by applying a saturating flash to a replicate leaf sample which had been stored in the dark for several hours. The modulation frequency of the fluorescence measuring beam was 100 kHz (1.3 μmol photons m^{-2} s^{-1}) except during measurements of the steady state F_o when the frequency was 1.6 kHz (0.04 μmol photons m^{-2} s^{-1}). Imposition of a weak far red background illumination (Schott RG9 filter) so as to ensure complete conversion of Q_A to the oxidized state during determinations of F_o (24) did not result in significant change in fluorescence yield compared to total darkness in these experiments. Irradiances reported herein were measured as the photon flux rate of visible light (400–700 nm) using a Li-Cor model LI 185-B quantum meter (Lincoln, NE).

Data Acquisition and Control

Analog IRGA and Fluorometer outputs were digitized by a DAP 1200/3 interface board (Microstar Laboratories, Redmond, WA) and stored in a Compaq 286 computer.

RESULTS

Effects of O_2 Concentration on Quantum Efficiency and Fluorescence Quenching

Quantum efficiency of photosynthesis (Φ_s) is expressed as mol CO_2 fixed: mol incident photons. Thus, quantum efficiency as used here should not be confused with limiting or intrinsic quantum efficiency obtained from the slope of the linear response to low photon flux rates (*i.e.* <300 μmol photons m^{-2} s^{-1}). Examples of changes in Φ_s and fluorescence quenching when irradiance is varied at a gas phase [O_2] of 1% (v/v) are shown for intact leaf tissue from tobacco (Fig. 1). The decline in Φ_s with increasing irradiance is accompanied by a nearly parallel decline in q_Q and a modest rise in q_{NP}. Cumulative results of several similar experiments in which irradiance and intercellular [CO_2] were varied are presented in Figure 2. A plot of changes in q_{NP} for the same experiments (Fig. 2, top) indicates that increases in Φ_s are associated with a decline in nonphotochemical quenching. Neither quenching coefficient alone serves as a simple and accurate means of predicting Φ_s.

When the values of Φ_s from Figure 2 were plotted *versus* associated ratios of q_Q:q_{NP} a highly significant ($P < 0.001$) linear relationship was noted (Fig. 3). Also shown in Figure 3

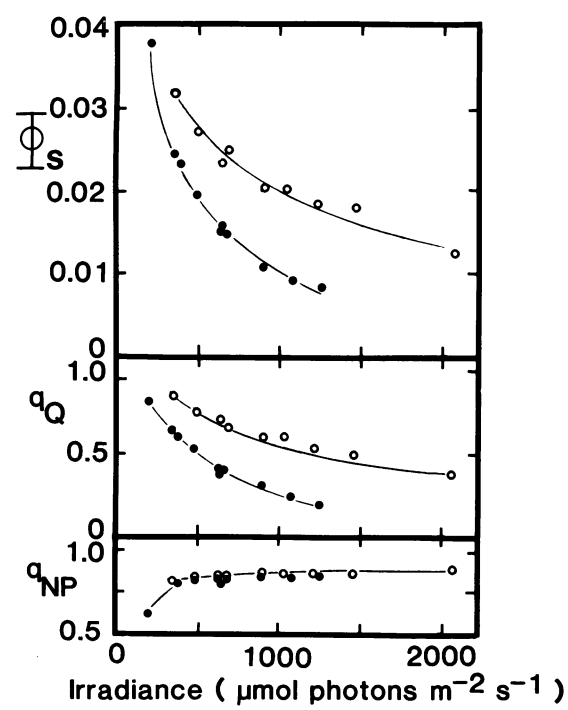

Figure 1. Representative examples of the dependence of quantum yield (Φ_s, top panel), q_Q (middle panel), and q_{NP} (bottom panel) on irradiance for leaf discs of tobacco at 25°C. The intercellular CO_2 concentrations were maintained at approximately 150 (●) and 390 (○) μbars and the [O_2] was 14 mbars. In these experiments irradiance was progressively lowered starting with the highest level shown.

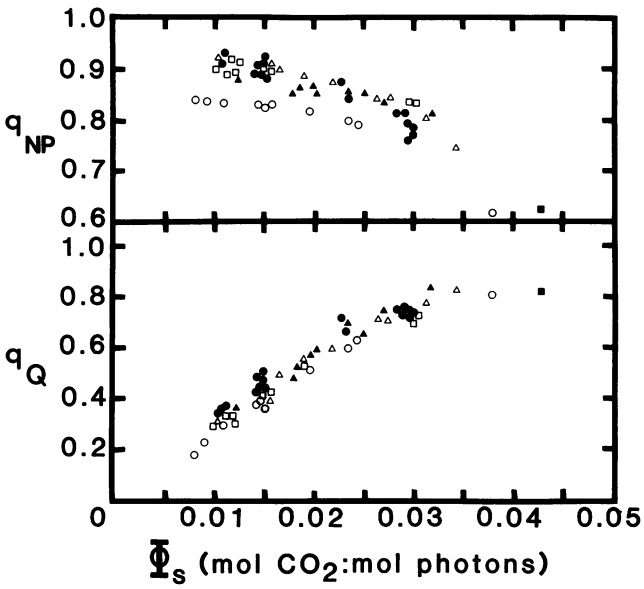

Figure 2. Changes in q_{NP} (top) and q_Q (bottom) with the quantum efficiency of net photosynthesis (Φ_s) at 1% O_2. Key to symbols: intercellular [CO_2] held at approximately 150 (○), 200 (△), 390 (▲), and 400 (■), μbars and irradiance varied; (●), intercellular [CO_2] varied at irradiances of 880 and 2100 μmol photons m^{-2} s^{-1}; (□), values of Φ_s measured at 1% O_2 and various C_i levels at the end of experiments in which [CO_2] and irradiance were varied at either 20.5 or 42% O_2.

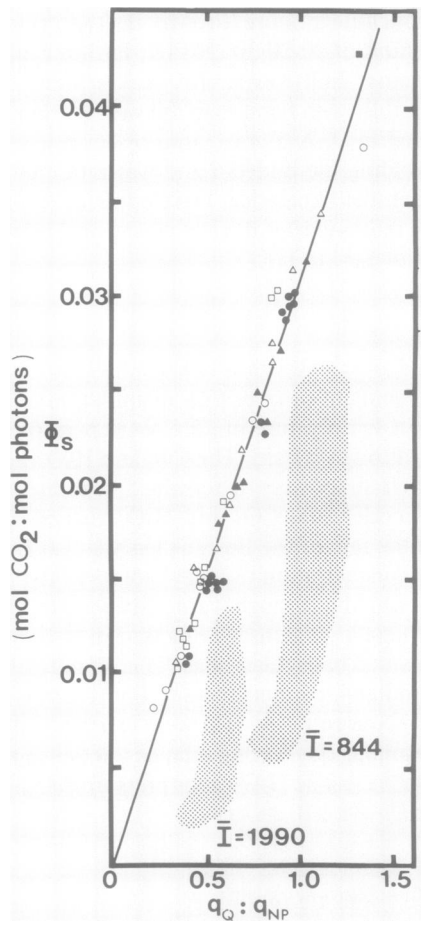

Figure 3. Relationship between Φ_s and q_Q:q_{NP} for the data shown in Figure 1. The straight line is the linear regression fit to the data (slope = 3.109×10^{-2}, y-intercept = 5.94×10^{-5}, correlation coefficient = 0.987, $P < 0.001$). The stipled areas delineate regions occupied by ordered pairs (Φ_s, q_Q:q_{NP}) obtained at 20.5% O_2 or 42% O_2 and the mean irradiances ($\bar{I}$) shown.

are regions of the Φ_s *versus* q_Q:q_{NP} plane occupied by data points obtained in the presence of 20.5% or 42% O_2 at the two mean irradiances shown. The molar ratio of intercellular [O_2]:[CO_2] was varied from 18 to 99 in these experiments. Nevertheless, irradiance interacts strongly with the [O_2]:[CO_2] ratio regarding the dependence of Φ_s on q_Q:q_{NP} such that two nonoverlapping regions could be discerned in Figure 3.

Partitioning of Noncyclic Photosynthetic Electron Transport

For the experiments performed at low [O_2] (*i.e.* 1% v/v) in Figures 2 and 3, noncyclic photosynthetic electron transport may be assumed to be quantitatively devoted to reduction of CO_2 provided externally (4 e^-:CO_2). Thus, associated values of Φ_s could be alternatively expressed in terms of the quantum efficiency of noncyclic electron transport ($\Phi_{se} = \Phi_s \times 4$). Furthermore, one may reasonably assume that the ultimate mode of utilization of photosynthetically produced reductant need not alter the relationship between PSII quantum efficiency and q_Q:q_{NP}. The predicted quantum efficiency of total noncyclic electron transport (Φ'_{se}) at elevated [O_2] is simply four times the value obtained by substitution of the observed q_Q:q_{NP} into the regression equation shown in the legend to Figure 3. The predicted rate of total noncyclic electron transport (μmol e^- m^{-2} s^{-1}) is Φ'_{se} times the irradiance. Likewise, the rate of noncyclic electron flow collectively expended in dissipative processes such as photorespiration and the Mehler reaction is the difference between the total rate and that supporting net CO_2 fixation (*i.e.* 4 × net CO_2 uptake rate).

Figures 4 and 5 illustrate changes in the partitioning of noncyclic electron transport as the C_i is varied at two irradiance levels and 20.5% or 42% O_2. At 20.5% O_2 the total electron transport rate increases by 50% over the range of C_i values examined. In contrast, at 42% O_2 the total rate remains relatively constant. As would be expected, maximal rates of total electron transport achieve higher levels at the higher irradiance employed. Rates of electron transport coupled to dissipative processes decline over this range of C_i values. At the higher C_i levels examined, the rate of dissipative electron transport still accounts for 25 to 35% of the total. Also shown in Figures 4 and 5 are the values of q_Q and q_{NP} measured in conjunction with net CO_2 uptake. The value of q_Q increases and q_{NP} declines somewhat with increasing C_i. The strong effect of irradiance on the magnitude of q_Q is evident.

Relative changes in partitioning of total noncyclic electron transport may be examined by defining (a) the proportion of electron flow allocated to net fixation of CO_2 as P_{net} and (b) the proportion diverted to dissipative processes as P_{diss} such that $P_{net} + P_{diss} = 1$. Furthermore, $P_{diss} = (\Phi'_{se} - \Phi_{se})/\Phi'_{se}$. Figure 6 shows the decline in P_{diss} as the C_i increases. At 20.5% O_2 (213 mbars) the irradiance level does not interact appreciably with C_i with regard to P_{diss}. However, at 42% O_2

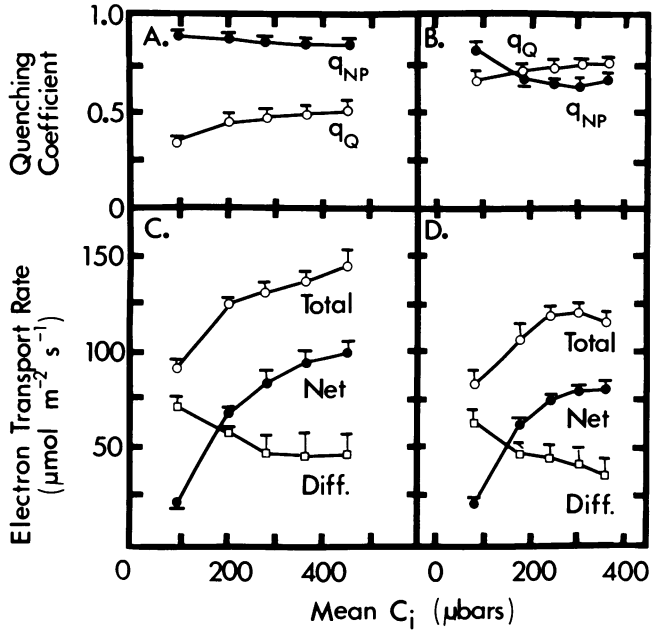

Figure 4. Fluorescence quenching (panels A and B) and partitioning of noncyclic photosynthetic electron transport versus the C_i (panels C and D) at 20.5% O_2 (213 mbars). The experiments were performed at two mean irradiance levels, 1943 (panels A and C) and 829 μmol photons m^{-2} s^{-1} (panels B and D). Each point is the mean of triplicate determinations and error bars indicate 1 SD. Total gas phase conductance to H_2O declined with increasing $[CO_2]$ and ranged from 0.45 to 0.25 mols m^{-2} s^{-1} at the high irradiance and from 0.33 to 0.13 mols m^{-2} s^{-1} at the low irradiance.

(439 mbars) P_{diss} is generally 10% greater at the higher irradiance over the range of C_i values examined.

DISCUSSION

Numerous studies have sought to account for gas exchange *in vivo* in terms of the kinetics of Rubisco. The reduction in the limiting quantum yield of CO_2 fixation in 21% O_2 relative to 1 to 2% O_2 and the progressive reversal of this effect as the dissolved O_2:CO_2 ratio decreases (5, 16) are consistent with predictions based on biochemical models (6, 21). Ehleringer and Björkman (5) reported an increase in limiting quantum yield with decreasing temperature in C_3 leaves. This effect of temperature persisted even when the quantum yields were adjusted to compensate for temperature-dependent changes in the relative solubilities of O_2 and CO_2. This is in accordance with the observed temperature response of Rubisco *in vitro* (13, 17). It should be noted, however, that Ku and Edwards (16) found only a slight residual temperature dependence in the inhibition of quantum yield by O_2 in wheat (C_3) after compensation for differential gas solubilities. Both studies reported no effect of elevated O_2 or temperature on limiting quantum yield in leaves of maize (C_4) which exhibit minimal photorespiration due to an efficient CO_2-concentrating mechanism in the bundle sheath cells where Rubisco is localized. Last, the O_2-dependence of photosynthetic $^{18}O_2$ uptake in C_3 leaves and inhibition of this process by CO_2 has been interpreted in terms of the oxygenase function of Rubisco and the role of O_2 in glycolate metabolism (3).

The Rubisco model, as set forth by Ogren and co-workers (13, 17), is

$$v_c/v_o = K_{sp} \cdot [CO_2]/[O_2] \quad (1)$$

where v_c/v_o is the ratio of the enzyme-catalyzed rates of carboxylation:oxygenation of RuBP. The constant K_{SP}, termed the 'specificity factor' (13), is equal to V_cK_o/V_oK_c where V_c and V_o are maximal velocities and K_c and K_o are Michaelis constants for carboxylation and oxygenation, respectively. The $[CO_2]/[O_2]$ is the ratio of the molar concentrations of these dissolved gases at the enzyme active site.

Metabolic sequences and associated stoichiometries for recycling of glycolate carbon have been reviewed (17, 21, 25). The first step in photorespiration is the oxygenation of RuBP whereby RuBP → glycolate-P + PGA (19). Two molecules of glycolate-P are ultimately metabolized to one each of PGA and CO_2. This stoichiometry tentatively assumes that metab-

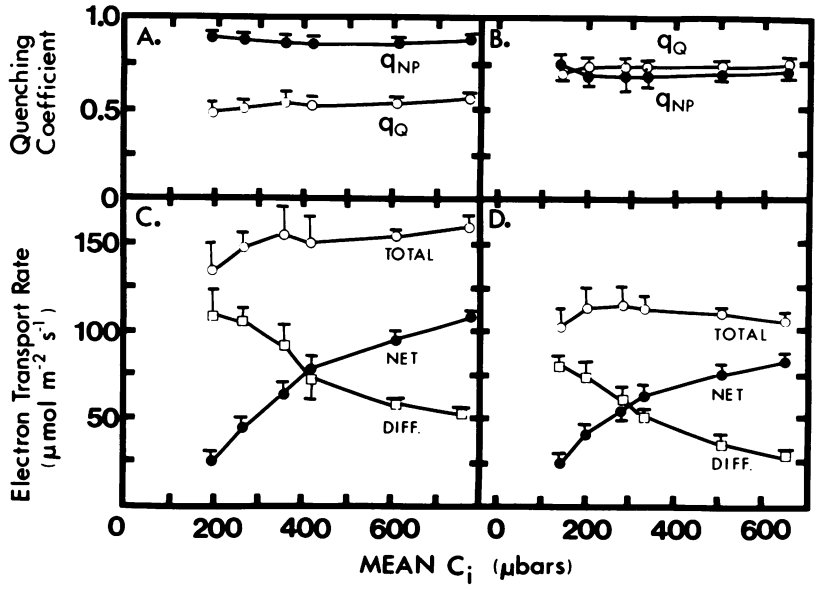

Figure 5. Fluorescence quenching and partitioning of noncyclic photosynthetic electron transport *versus* the C_i at 42% O_2 (439 mbars). The mean irradiance levels were 2018 (panels A and C) and 852 μmol photons m^{-2} s^{-1} (panels B and D). Total gas phase conductances to H_2O ranged from 0.35 to 0.18 mols m^{-2} s^{-1} at the high irradiance and from 0.24 to 0.11 mols m^{-2} s^{-1} at the low irradiance. See legend to Figure 4 and text for further information.

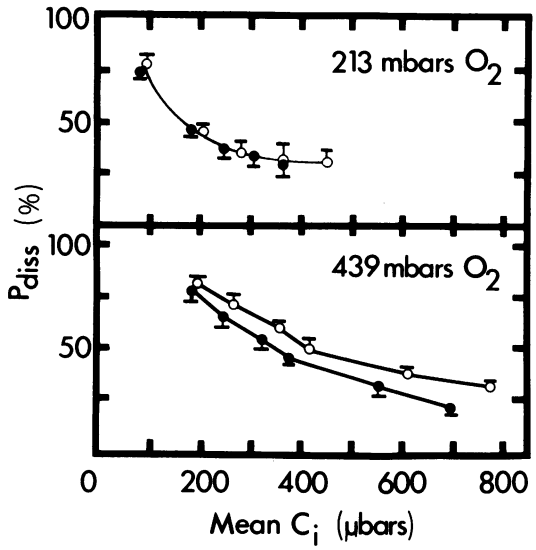

Figure 6. Plots of photosynthetic electron allocation (P_{diss}) factors versus the mean C_i for the two O_2 levels shown in the panels. The values are calculated from the data of Figures 4 and 5 and points obtained at high irradiance (○) are differentiated from those obtained at the lower irradiance (●). Error bars indicate 1 SD.

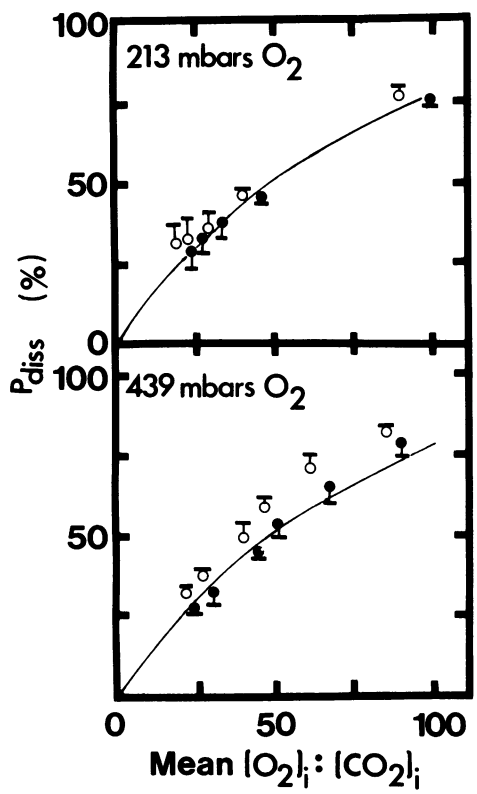

Figure 7. Relationship between P_{diss} and the molar ratio of intercellular $[O_2]$:$[CO_2]$ for the data shown in Figures 4 and 5. Alpha values used in computing molar concentrations of these gases obtained from Hodgman and Lange (11). Presentation of the data regarding independent effects of $[O_2]$ and irradiance is as in Figure 6. The solid lines are rectangular hyperbolae obtained from Eq. 3 (see text) using a value for K_{sp} of 95. Error bars indicate 1 SD.

olism of glycolate-P proceeds through the glycine → serine conversion located in the mitochondrion resulting in release of 25% of the glycolate carbon as CO_2. Thus, for two oxygenations, three molecules of NADPH are required to reduce the three molecules of PGA to triose phosphate. Two molecules of NADPH are needed to refix each photorespired CO_2. Finally, an additional two equivalents of reduced ferredoxin are required by the glutamine synthetase-glutamate synthase sequence for reassimilation of the NH_3 released during the glycine → serine conversion. Overall, 12 low potential electrons are consumed for every two glycolate-P molecules metabolized. Therefore, the rate of noncyclic photosynthetic electron transport coupled to photorespiration is 6 v_o. If v_{ca} is the rate of net uptake of CO_2 by the leaf, then allocation of electron flow to photorespiration relative to the total noncyclic electron transport rate is

$$P_{diss} = 6\ v_o/(4\ v_{ca} + 6\ v_o). \quad (2)$$

Since $v_c = v_{ca} + 0.5\ v_o$, using equation 1, v_o may be expressed in terms of v_{ca} such that $v_o = (v_{ca} \cdot [O_2]/[CO_2])/(K_{sp} - 0.5 \cdot [O_2]/[CO_2])$. Substitutions of this last expression into Eq. 2 yields

$$P_{diss} = 1.5 \cdot ([O_2]/[CO_2])/(K_{sp} + [O_2]/[CO_2]) \quad (3)$$

which is the formula for a rectangular hyperbola.

Figure 7 (solid lines) shows the predicted dependence of P_{diss} on the $[O_2]$:$[CO_2]$ ratio for $K_{sp} = 95$. Also shown are the data from Figure 6 plotted *versus* the intercellular molar ratio of $[O_2]$:$[CO_2]$. Within the limits of experimental error the points fall along the Rubisco simulation except at 439 mbars O_2 and high irradiance (Fig. 7, bottom). These latter data will be discussed later.

The value for K_{sp} of 95 employed in Figure 7 is well within the range of values reported for Rubisco at 25°C. Jordan and Ogren (13) published values for isolated enzymes from C_3 plants which ranged from 77 to 88. Brooks and Farquhar (2) reported values of 101.6 and 94.1 for wheat and spinach leaves, respectively, using a modified CO_2 compensation point assay. These authors also analyzed the *in vitro* data of Hall and Keys (8) obtained with the wheat enzyme and calculated a K_{sp} of about 112. It is not possible to conclude whether these reported variations in K_{sp} are indicative of a true plasticity in this quantity or merely represent biases inherent in the different methods of estimation. For instance, as discussed in Brooks and Farquhar (2) the actual $[CO_2]$ in the chloroplast may differ from the intercellular $[CO_2]$ when using *in vivo* approaches such as the one described here. The chloroplast $[CO_2]$ may be reasonably expected to be somewhat lower than the intercellular $[CO_2]$ due to mesophyll resistance to diffusion of CO_2 which is likely to be considerably smaller than the stomatal resistance. If this quantity were known, use of the chloroplast $[CO_2]$ in Figure 7 would result in a probable slight shift of the data points to the right. Thus, the value for K_{sp} of 95 employed here represents a minimal estimate of the true value *in vivo* assuming, of course, that the magnitude of K_{sp} is indeed invariant.

Use of Eq. 1 and $K_{sp} = 95$ enables calculation of the CO_2 compensation concentration (*i.e.* $P_{diss} = 1.00$) for the two levels of O_2 shown in Figure 7. These are 42 and 86 μbars CO_2 for 213 and 439 mbars O_2, respectively. These values are

compatible with previous estimates of the CO_2 compensation point for C_3 plants at 25°C (2, 13). The values of C_i in equilibrium with an external [CO_2] of 350 μbars and 213 mbars O_2 at the high and low irradiances of Figure 6 (top) are 261 and 231 μbars, respectively. Substitution of equivalent molar CO_2 concentrations (α values for CO_2 and O_2 are 0.759 and 0.02831, respectively, at 25°C, see ref. 11) into Eq. 1 indicates that the ratios of photorespiratory CO_2 evolution:net CO_2 uptake are 19.1 and 22.1%, respectively, under these conditions.

Comparison of observed results with predictions based on the Rubisco model have so far assumed that the fraction of glycolate carbon which is photorespired remains fixed at 25%. Evidence from this laboratory has been presented suggesting that the stoichiometry of photorespiration may sometimes substantially exceed 25% (9). This may account for the results obtained at 439 mbars O_2 and high irradiance (Fig. 7, bottom) in which observed P_{diss} values significantly exceeded predictions based on the Rubisco model and $K_{sp} = 95$. For instance, peroxidation of photorespiratory hydroxypyruvate would increase the CO_2 evolved:glycolate metabolized resulting in increased commitment of reducing equivalents (*i.e.* NADPH) to refixation of CO_2. Hence, a higher than expected P_{diss} value could result without changes in K_{sp} or the [O_2]/[CO_2]. Alternatively, these data may represent occurrence of Mehler-type processes in addition to photorespiration (10). Photoreduction of O_2 is associated with elevated O_2 levels and a relatively reduced ferredoxin pool (7). The level of reduction of ferredoxin will likely increase with irradiance due to enhanced PSI activity. It is impossible, given the data available, to distinguish between these two possibilities. Note that mitochondrial dark respiratory rates (~1 μmol CO_2 m^{-2} s^{-1}) are not likely to have a significant effect on the P_{diss} in these experiments and therefore its contribution has been neglected.

In conclusion, the results obtained by measurements of fluorescence yield and net CO_2 exchange provide support for the applicability of the Rubisco model over a wide range of CO_2 concentrations and at 25°C. Irradiance and [O_2] are sometimes capable of interacting to either alter the way by which glycolate is metabolized or to activate alternative pathways for O_2-dependent photosynthetic electron transport. This approach should enhance our understanding of how O_2 interacts with the intact leaf and aid in the search for plants with superior photosynthetic efficiency due to reduced photorespiration.

ACKNOWLEDGMENTS

I wish to thank Nancy Burns for skillful technical assistance and Israel Zelitch for helpful comments on the manuscript.

LITERATURE CITED

1. **Bradbury M, Baker NR** (1981) Analysis of the slow phases of the *in vivo* chlorophyll fluorescence induction curve. Changes in the redox state of photosystem II electron acceptors and fluorescence emission from photosystems I and II. Biochim Biophys Acta **635:** 542–551
2. **Brooks A, Farquhar GL** (1985) Effect of temperature on the CO_2/O_2 specificity of ribulose-1,5-bisphosphate carboxylase/oxygenase and the rate of respiration in the light. Planta **165:** 347–406
3. **Canvin DT, Berry JA, Badger MR, Fock H, Osmond CB** (1980) Oxygen exchange in leaves in the light. Plant Physiol **66:** 302–307
4. **Dietz K-J, Schreiber U, Heber U** (1985) The relationship between the redox state of Q_A and photosynthesis in leaves at various carbon-dioxide, oxygen and light regimes. Planta **166:** 219–226
5. **Ehleringer J, Björkman O** (1977) Quantum yields for CO_2 uptake in C_3 and C_4 plants. Dependence on temperature, CO_2, and O_2 concentration. Plant Physiol **59:** 86–90
6. **Farquhar GD, Von Caemmerer S, Berry JA** (1980) A biochemical model of photosynthetic CO_2 assimilation in leaves of C_3 species. Planta **149:** 78–90
7. **Furbank RT, Badger MR** (1983) Oxygen exchange associated with electron transport and photophosphorylation in spinach thylakoids. Biochim Biophys Acta **723:** 400–409
8. **Hall NP, Keys AJ** (1983) Temperature dependence of the enzymic carboxylation and oxygenation of ribulose 1,5-bisphosphate in relation to effects of temperature on photosynthesis. Plant Physiol **72:** 945–948
9. **Hanson KR, Peterson RB** (1985) The stoichiometry of photorespiration during C_3-photosynthesis is not fixed: Evidence from combined physical and stereochemical methods. Arch Biochem Biophys **237:** 300–313
10. **Heber U, Egneus H, Hanck U, Jensen M, Köster S** (1978) Regulation of photosynthetic electron transport and phosphorylation in intact chloroplasts and leaves of *Spinacia oleracea L.* Planta **143:** 41–49
11. **Hodgman CD, Lange NA** (1931) Solubility of gases in water. *In* RC Weast, ed. Handbook of Chemistry and Physics. Ed 16, Chemical Rubber Publishing Co., Cleveland, pp 570–571
12. **Horton P, Hague A** (1988) Studies of the induction of chlorophyll fluorescence in isolated barley protoplasts. IV. Resolution of non-photochemical quenching. Biochim Biophys Acta **932:** 107–115
13. **Jordan DB, Ogren WL** (1984) The CO_2/O_2 specificity of ribulose 1,5-bisphosphate carboxylase/oxygenase. Planta **161:** 308–313
14. **Krause GH, Laasch H** (1987) Energy-dependent chlorophyll fluorescence quenching in chloroplasts correlated with quantum yield of photosynthesis. Z Naturforsch **42c:** 581–584
15. **Krause GH, Vernotte C, Briantais J-M** (1982) Photoinduced quenching of chlorophyll fluorescence in intact chloroplasts and algae. Resolution into two components. Biochim Biophys Acta **679:** 116–124
16. **Ku S-B, Edwards GE** (1978) Oxygen inhibition of photosynthesis. III. Temperature dependence of quantum yield and its relation to O_2/CO_2 solubility ratio. Planta **140:** 1–6
17. **Laing WA, Ogren WL, Hageman RH** (1974) Regulation of soybean net photosynthetic CO_2 fixation by the interaction of CO_2, O_2, and ribulose 1,5-diphosphate carboxylase. Plant Physiol **54:** 678–685
18. **Long SP, Hallgren J-E** (1985) Measurement of CO_2 assimilation by plants in the field and the laboratory. *In* J Coombs, DO Hall, SP Long, JMO Scurlock, eds, Techniques in Bioproductivity and Photosynthesis, Ed 2. Pergamon Press, Oxford, pp 62–94
19. **Lorimer GH, Andrews TJ, Tolbert NE** (1973) Ribulose diphosphate oxygenase. II. Further proof of reaction products and mechanism of action. Biochemistry **12:** 18–23
20. **Mehler AH** (1951) Studies on reactions of illuminated chloroplasts. I. Mechanism of the reduction of oxygen and other Hill reagents. Arch Biochem Biophys **33:** 65–77
21. **Osmond CB** (1981) Photorespiration and photoinhibition. Some implications for the energetics of photosynthesis. Biochim Biophys Acta **639:** 77–98
22. **Peterson RB, Sivak MN, Walker DA** (1988) Relationship between steady state fluorescence yield and photosynthetic efficiency in spinach leaf tissue. Plant Physiol **88:** 158–163

23. **Schreiber U, Bilger W, Schliwa U** (1986) Continuous recording of photochemical and nonphotochemical quenching with new type of modulation fluorometer. Photosynth Res **10:** 51–62
24. **Weis E, Berry JA** (1987) Quantum efficiency of photosystem 2 in relation to 'energy' dependent quenching of chlorophyll fluorescence. Biochim Biophys Acta **894:** 198–208
25. **Zelitch I** (1971) Photosynthesis, Photorespiration and Plant Productivity. Academic Press, New York, pp 58–212